EMEP/MSC-W Note 2/97
Date: July 1997

emep

Co-operative programme for monitoring and evaluation of the long range transmission of air pollutants in Europe

Status of the development of the regional scale photo-chemical multi-layer Eulerian model.

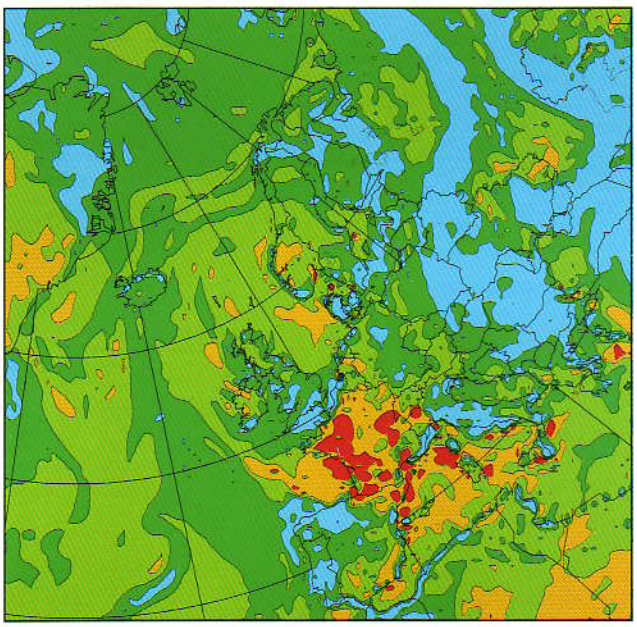

JAN E. JONSON,
HUGO A. JAKOBSEN AND
ERIK BERGE

msc-w

Meteorological Synthesizing Centre - West
the Norwegian Meteorological Institute
P.o. Box 43-Blindern, N-0313 Oslo 3, Norway

EMEP/MSC-W Note 2/97
Date July 1997

Status of the development of the regional scale photo-chemical multi-layer Eulerian model

by

Jan E. Jonson, Hugo A. Jakobsen and Erik Berge

Det Norske Meteorologiske Institutt
Research Report no. 52

ISSN 0332-9897

Contents

	Page
Preface and acknowledgements	3
1. Introduction	4
2. Model description	5
2.1 Chemistry	5
2.2 Dissociation rates	5
2.3 Dry and wet deposition	7
2.4 Advection	7
2.5 Emissions	9
3. Meteorological situation	11
4. Model validation	11
4.1 Snapshots of NO_2, VOC, O_3 and O_3 production	11
4.2 Time series for ozone	15
5. Comparisons with the MADE-50 model.	18
6. Low emission scenario	22
7. Summary and conclusions	22
8. References	23
Appendix	26

Preface and acknowledgements

This report was prepared to be presented at the twenty first session of the Steering Body of EMEP (Co-operative Programme for Monitoring and Evaluation of the Long Range Transmission of Air Pollutants in Europe). It provides a description of the regional scale Eulerian photooxidant model, model results and comparisons with measurements, and finally scenario calculations with reduced antropogenic emissions.

Basic input to the regional scale Eulerian model is meteorological data from a dedicated version of the routine Numerical Weather Prediction (NWP) model at the Norwegian Meteorological Institute (DNMI). Furthermore, basic input to the model include the emission fields, boundary values for the various compounds and photodissociation rates. The calculated results presented in this report are strongly dependant on this input and the authors want to thank the contributors for supplying the requested data and programming code.

The chemistry scheme presently applied in the model has been developed at the Department of Geophysics, University of Oslo. We wish to thank Professor Ivar S.A. Isaksen, Dr. Terje Berntsen and Jostein Sundet for providing the code and for valuable advice in implementing the code. The programming code and date files required for the calculation of natural emissions of isoprenes has been provided by David Simpson. We also want to thank David Simpson for his support in the development of this model version.

The model calculations have been performed on the Cray T3E parallel super computer with 96 processors at the Norwegian University of Science and Technology (NTNU) in Trondheim, Norway. The access to the computer is greatly appreciated. We will also acknowledge the support and help from Dr. Roar Skålin and Dr. Jørn Amundsen.

1. Introduction

Applying the same model concepts as for the MADE-50 model, a new version of the Eulerian multi-layer model has been developed. The development of the model is done in co-operation with the department of Geophysics, University of Oslo. The model, henceforth called the MACHO model (Multi-layer Atmospheric CHemistry model, Oslo), use the same set of components and reaction rates as in the global Oslo CTM1 (Berntsen, 1994; Berntsen et al., 1997). The development of the MACHO model falls within the EMEP/MSC-W strategy for a shift from single-layer Lagrangian models, to more complex Multi-layer Eulerian models. With the MACHO model photo-oxidant chemistry, including ozone formation in the troposphere, is described within the framework of the Multi-layer model.

For several applications, such as calculations of source receptor relationships for acidifying components, calculations will be made with the much simpler MADE-50 model also in the future. The MACHO model will also serve as a tool, improving our understanding of the chemical processes parameterized in the MADE-50 model. It is our hope that a better understanding of the processes involved in the turnover of sulphur and nitrogen species learned from the MACHO model will result in improvements in the parameterization of the same processes in the MADE-50 model.

At EMEP/MSC-W ozone in the boundary layer is calculated with a single layer Lagrangian model. The physical structure of this model (advection and meteorological algorithms etc.) are based on the ROOT-150 model (Barret et al., 1995). The chemistry is an updated and extended version of the so called Norwegian Trajectory Model (Eliassen et al. 1982; Hov et al., 1985).

Although different, the chemistry schemes applied in the Lagrangian ozone model and the MACHO model (and the Oslo CTM1) are of common origin. The MACHO model includes the chemistry of 45 components whereas close to 70 are included in the Lagrangian ozone model. A major difference in the two schemes is the complexity in the description of the degradation chain of isoprenes. In the Lagrangian ozone model 18 components are included in the degradation scheme (Simpson et al., 1995) as opposed to only 4 in the MACHO model. For the MACHO model the chemistry parameterization from the Oslo CTM1 was selected in order to reduce the amount of computing resources used by the model. Also, for the Department of Geophysics, University of Oslo, it has been a point to have a coherent chemistry parameterization, in particular for calculations in the upper troposphere, where concentrations are critically dependant on lateral boundary conditions. Lateral boundary conditions will in the future be supplied by the Oslo CTM2, an updated version of the Oslo CTM1 with modular horizontal resolution using meteorological input data from the ECMWF.

At EMEP/MSC-W 1992 has been selected for extensive studies of depositions and concentrations of acidifying components, applying the MADE-50 model (Jakobsen et al., 1997). In order to avoid additional storage of meteorological data, 1992 is selected also for the modelling of photochemical chemistry.

In the late spring and summer months ozone concentrations are typically in the 30 to 50 ppb range (Hjellbrekke, 1995). However, in fair weather situations ozone in the boundary layer may reach levels that may cause health problems (Delfino et al., 1996). By U.S. EPA. (1996) ozone is considered the pollutant of greatest concern with respect to the potential regional impact to threes.

Hourly surface measurements of O_3, have been made on a routine basis for a number of locations within the EMEP network for several years. For NO_2 (an important ozone precursor) and HNO_3 model results can be compared to measurements as demonstrated with the MADE-50 model (this years report) and the ROOT models (Barret et and Berge, 1996). These measurements can be supplemented by additional measurements (i.e. as part of the TOR project within EUROTRAC). In this report modelled ozone will be compared to the EMEP measurements. Modelled results for NO_2 and HNO_3 will also be compared to measurements.

2. Model Description:

The basic model architecture of the MACHO model is the same as that of the MADE-50 model (Jakobsen et al. 1995, 1996 and 1997). However, altogether 45 chemical components are included in the MACHO model, of which 39 are advected, whereas the MADE-50 model includes chemistry and advection of 9 components only.The chemistry has been applied in the Oslo CTM1, a global 3D chemical tracer model at the University of Oslo. Monthly averaged initial values and boundary values are also provided by the Oslo CTM1. For remote areas ozone is in general underpredicted by the Oslo CTM1. For ozone a lower limit of 40 ppb is assumed for initial and boundary values.

2.1 Chemistry

The chemical mechanism applied in the model is virtually identical to the one presently applied in the Oslo CTM1 (Berntsen et al., 1994, Berntsen and Isaksen, 1997). The chemistry scheme is similar to the one presently used in the lagrangian ozone model (Malik et al., 1996). The scheme includes 110 thermal reactions and 17 photolytic reactions. (Appendix). The coupled set of differential equations in the is solved by a quasi steady-state approximation method (QSSA), with iterations for the short-lived components (Hesstvedt et al., 1978). A simplified scheme for the oxidation of isoprenes is also included in the calculations.

2.2 Dissociation rates.

Dissociation rates for clear sky conditions, and for two predefined clouds, are calculated with the DISSORT routine (Kylling, 1995). In the calculations seasonal ozone concentrations from a 2D model (Stordal et al. 1985) are scaled by zonally and monthly averaged observations of total ozone columns (Dusch, 1974). Clear sky dissociation rates are calculated for every 10 degrees latitude and for every integer zenith angle. At every time step and every grid box location the nearest rate is selected with respect to solar zenith angle and geographical position. In addition, dissociation rates at 55 degrees north are calculated for two predefined clouds for every integer zenith angle. Cloud base for both the predefined clouds are at 1 km altitude. Cloud 1 is 3 km deep, with a water content of 0.7 g m^{-3} and mean droplet radius of 10 μm,

whereas cloud 2 is 1 km deep with a water content of only 0.3 g m^{-3} and mean droplet radius of 6 μm. Dissociation rates for the photolytic reaction:

$$O_3 + h\nu \text{---> } O_2 + O'D$$

at 55 degrees north for clear sky condition and for the two cloud types are shown in Figure 1 for may 15'th. Compared to clear sky conditions, dissociation rates are increased above the clouds by reflection from the underlying clouds. Within the clouds, dissociation rates are increased by multiple scattering between the droplets, but as the distance from cloud top increase, the scattering results in a decrease in the dissociation rates. Below the clouds dissociation rates are markedly lower than the corresponding clear sky rates.

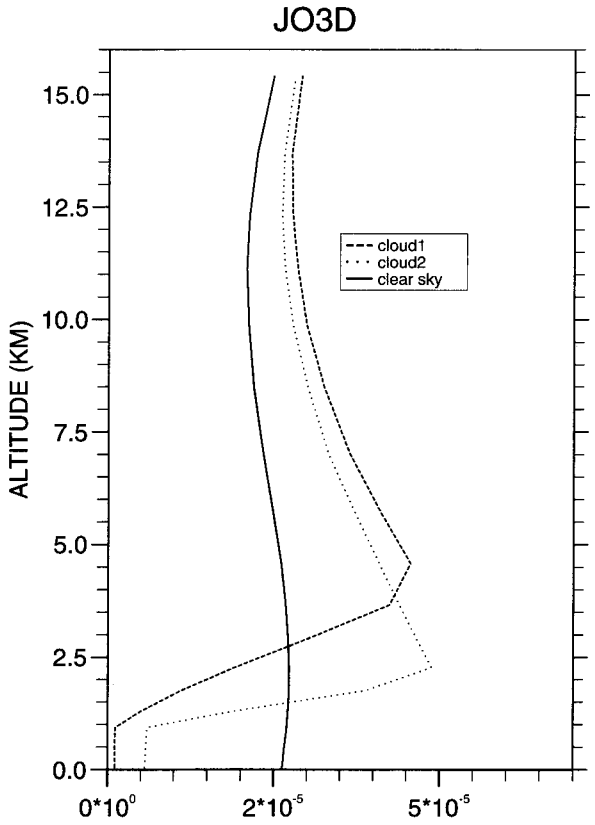

Figure 1 Photolysis of ozone ($O_3 + h\nu$---> $O_2 + O'D$) at 55 degrees north for clear skies and fo two cloud types (see text).

Table 1: Dry deposition at 1 m in $cm \cdot s^{-1}$

	O_3	HNO_3	PAN	CO	H_2O_2	NO_2
Ocean	0.1	0.1	0.	0.	0.1	0.05
Ice	0.05	0.05	0.	0.	0.01	0.02
Tundra	0.1	0.1	0.05	0.01	0.1	0.05
Agriculture	0.4	0.4	0.2	0.03	0.1	0.1
Forest	0.4	0.4	0.2	0.03	0.1	0.1
Desert	0.1	0.1	0.05	0.01	0.1	0.05
Undefined	0.4	0.4	0.2	0.03	0.1	0.1

2.3 Dry and wet deposition

The dry deposition parameterization scheme applied here is used in former versions of the MADE-50 model (Berge, 1993; Jakobsen et al. 1995). The dry deposition velocities at 1 m (v_{1m}) are given in Table 1. Effective dry deposition velocities for the lowest model layer (v_{eff}) are calculated based on the vertical diffusion coefficient (Berge, 1993) from the equation:

$$v_{eff} = \frac{v_{1m}}{\left[1 + \frac{v_{1m}}{C_D |V_{45m}|}\right]}$$

where C_D is the drag coefficient and $\mathbf{V}_{45m}$ is the wind speed in the lowest model level.

Presently only HNO_3 and H_2O_2 are removed by wet scavenging. The wet scavenging is calculated locally in each layer as a product of the precipitation rate, the local concentration, a characteristic scavenging depth (1000 m) and a scavenging ratio. For in-cloud scavenging the scavenging ratio is 10^6 and $7 \cdot 10^5$ for HNO_3 and H_2O_2 respectively. Below cloud base the scavenging ratio is reduced by a factor of two. The parameterization of wet scavenging is described in more detail in Berge (1993).

2.4 Advection

The basic model equation is described in previous reports on the Eulerian multi-layer model (e.g. Jakobsen et al., 1995). As in the MADE-50 model (Jakobsen et al., 1996) an implicit

upwind scheme is used for the vertical advection, whereas an explicit 4'th order Bott scheme is applied for the horizontal advection (Bott, 1989a,b).

It is well known (e.g. Bott, 1992 and 1993; Easter, 1993) that the time split numerical form of the advection part of the equation may become unstable for deformational flows because it does not properly account for the non-zero components of the divergence during each one-dimensional transport step. According to Easter (1993), this is because one step of the time-splitting solution will decrease (or increase) the concentration in a grid cell, and the following steps in the other two directions should increase (or decrease) the concentration in a compensating manner, but the three changes do not exactly balance due to the intermediate or temporary concentration fields applied for the advection in the latter two directions. The numerical instabilities described above may however interact with other numerical modes occurring in the air pollution models. The origin of such artificial modes may for example include inaccurate non-linear numerical responses in the chemistry scheme, and stiffness problems related to the solution of the chemistry model equations due to large varieties in lifetimes of the different chemical species involved. Furthermore, non-monotonic advection algorithms may overestimated (or underestimate) the numerical responses due to large gradients in the emission estimates. The coupling of such numerical instabilities depends heavily on the model complexity. Therefore, compared to the numerical problems handled solving the simpler MADE-50 model, the numerical task solving the MACHO model equations requires improved algorithms since this model contains a full photo-chemistry scheme were the numerical equations are more involved containing amplified couplings of the numerical instability modes.

To handle the instabilities associated with deformational flows, an alternate time-splitting approach based on the method of Easter (1993) is used here. Our method solves

$$\frac{\partial}{\partial t}(\psi p^*) = -m^2 \nabla_H \bullet \left(\frac{V_H}{m} \psi p^* \right) - \frac{\partial}{\partial \sigma}(\dot{\sigma} \psi p^*)$$

in conjunction with

$$\frac{\partial}{\partial t}(p^*) = -m^2 \nabla_H \bullet \left(\frac{V_H}{m} p^* \right) - \frac{\partial}{\partial \sigma}(\dot{\sigma} p^*)$$

where Ψ is the mixing ratio, $p^* = p_s - p_{tot}$, where p_s is the surface pressure and p_{tot} is the pressure at the top of the model atmosphere (= 100 hPa). t and σ is the time and vertical coordinates, respectively. $\dot{\sigma}$ is the vertical velocity, m is the map factor on a polar stereographic map projection, $\mathbf{V}_H$ is the wind vector, and ∇_H is the del operator.

The basis of this approach is that during each one-dimensional transport step of the time-split algorithm, a positive (or negative) component of divergence will temporarily decrease (or increase) the mass of both fluid and tracer in a grid cell, but the tracer mixing ratio should physically only change as a result of advection along tracer gradients. The net fluid-mass change after transport in all directions should be equal to the time dependency of the pressure

in accordance with the total fluid continuity equation (i.e. if the fluid continuity equation is fulfilled) because of compensating divergence components in the different coordinate directions. Solving these two equations together allows one to eliminate net tracer mass changes due to fluid deformation, and thereby eliminate the instability in deformational flows.

In addition, in both multi-layer models similar numerical instabilities can arise in these transport calculations if the meteorological input data (e.g. wind, temperature and pressure) do not accurately conserve mass due to limitations in the numerical schemes implemented in the numerical weather prediction (NWP) model, or due to inaccurate and insufficient mass conserving properties of the interpolation algorithms applied to the off-line forecast data. To keep track of the actual mass in the system, the total fluid continuity equation should thus be solved prognostically initiated at the start of the simulation only. Comparing the actual pressure fields obtained from the NWP-model and the adjusted fields found by resolving the total fluid continuity equation, will give a measure of the accumulated imbalance in the input data. Unfortunately, we do not have time for any detailed analysis of this matter this year so this important numerical exercise is left for future work. At present, as a first approach, the pressure obtained by resolving prognostically the total fluid continuity equation is initiated every time step in the simulation to avoid any possible numerical difficulties related to the linear time interpolation of the meteorological data applied to the air pollution model between the 6-hourly forecast data sets available (see Jakobsen et al., 1995). In these time intervals, there are no algorithm implemented actually ensuring that the total mass of air in the calculating domain is really conserved and thus not artificially increased or decreased by this numerical interpolation procedure. However, the same time interpolation algorithm has been used for the MADE-50 calculations for which the code actually monitors the mass budgets, and to date only minor numerical sinks and sources are detected for time series up to one year.

2.5 Emissions

Surface emission field estimate for antropogenic NO_x, CO and VOC (Volatile Organic Compounds) are based on data submitted officially to EMEP from the participating countries. Gridded data are available from many countries in the 50 km EMEP grid. A distinction is made between surface sources (below 100 m) and high stack sources (above 100 m).

Monthly averaged lightning emissions on a T21 resolution from Köhler et al. (1995), and seasonally averaged aircraft emissions on a T42 resolution from the ANCAT 2 database, provided by the EU project POLINAT 2 (Gardner et al., 1997), are also included. However the two latter sources have virtually no effects on surface concentrations over Europe.

Natural emissions of isoprenes are calculated as described by Simpson et al. (1995). Different source strenghts are assumed for different types of vegetation cover. The vegetation classification described by Simpson et al. (1995) on a 150 km resolution is used. For oaks, emission factors are split between northern European oaks (high emitters) and southern European oaks (generally low emitters). Likewise emission factors for spruce trees are split between low emitters and moderately high emitters (e.g. Sitka Spruce).

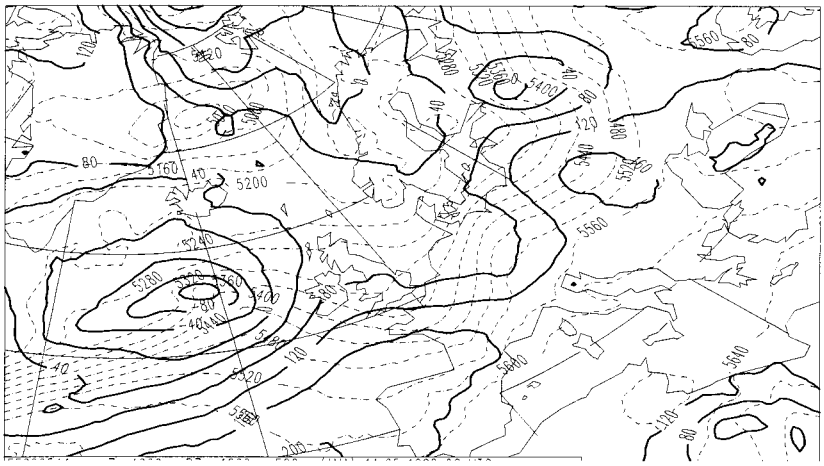

may 11'th 1992 12 UTC

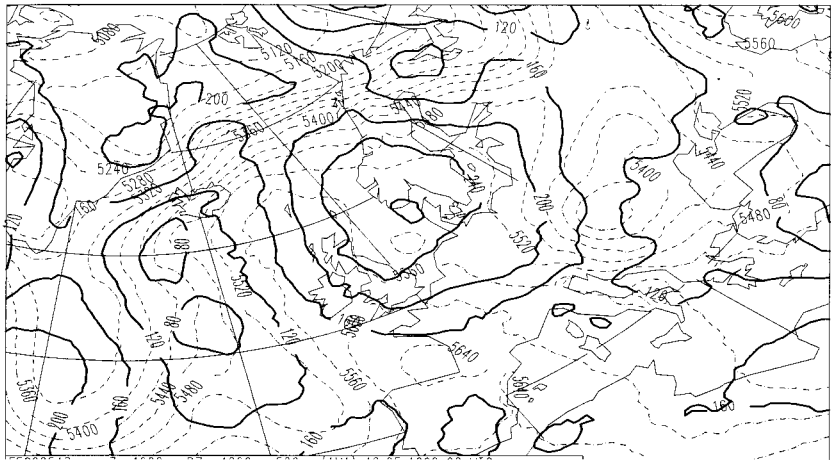

may 18'th 1992 12 UTC

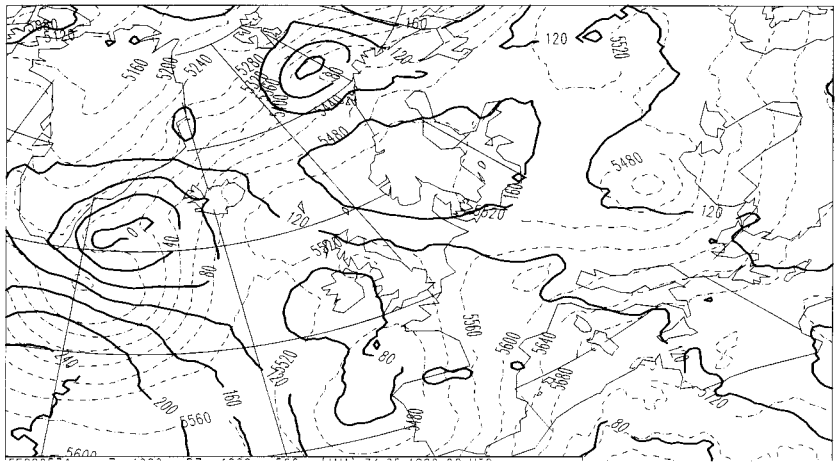

may 31'th 1992 12 UTC

Figure 2 Geopotential height in meters of the 1000 hpa surface (thick lines), and the height in meters between the 500 and 1000 hpa surfaces (thin lines).

3. Meteorological situation

With regard to weather patterns and to photochemical production of ozone in northern Europe, May 1992 can roughly be divided into two parts, before and after May 13'th. The first part of the month was dominated by several low pressure systems passing over Northern Europe, giving cool and cloudy weather with westerly winds. As an example Figure 2 (top panel) depicts the situation at noon may 10'th. An extensive low pressure system is situated over northern Scandinavia. Northwestern parts of Europe is experiencing westerly winds, cool and cloudy weather with some rain. Relatively clean background air is advected in from the Atlantic. The conditions does not favour photochemical activity and subsequent buildup of additional ozone in NW and central Europe.

The second period (from around May 13'th and the rest of the month) was characterized by a blocking high pressure system over northern Europe. The situation is illustrated in Figure 2 (middle and lover panel) depicting the situation at noon may 18'th and may 31'th respectively. Both at may 18'th and may 31'th a high pressure system is situated over southern Scandinavia. However, at may 31'th a low pressure system is situated over Ireland and west of Spain, and the high pressure system is beginning to break down over central Europe

4. Model validation.

In this section model results for several components are depicted as snapshots in the lowest model layer (approx. 45 m). Furthermore, model results for O_3, NO_2 and HNO_3 are compared to measurements. In the comparison, the main focus will be on ozone.

4.1 Snapshots of NO_2, VOC, O_3 and O_3 production

In Figures 3 - 5 ozone concentrations in the lowest model layer (approx. 45 m) are depicted at 12 UTC for the same 3 days as for the meteorological situations shown in Figure 2.

In Figure 3 ozone concentrations on May 11'th are shown. High ozone levels are found in and around the Mediterranean ocean. Throughout the rest of Europe ozone levels are in general low. This is in good agreement with what can be expected from the meteorological situation in the first part of the month, as described in section 3 above.

On may 18'th ozone concentrations are high also in western Europe (Figure 4). As shown in Figure 2, middle panel, the general wind direction in central Europe is from the east. As ozone precursors (NO_x and VOC), emitted in central Europe, are advected west ozone is produced, giving high ozone concentrations, in particular over western parts of France. As ozone and ozone precursors are advected west, then north across the British Isles and finally towards western Norway, ozone is produced, giving relatively high ozone values also in western parts of Scandinavia. The net production of ozone in the lowest model layer at 12 UTC may 18'th is

visualized in Figure 6. In Figures 7 and 8 the concentrations of NO_x and VOC respectively, are shown for the same time as for ozone and net ozone production. For both components the plume from central Europe, across the British Isles towards western Norway, as discussed above, is clearly visible. The highest net ozone production is found slightly south and west of the main pollution plume. In northern parts of France, and over England ozone is destroyed by the high NO_x concentrations.

Finally, on may 31'th, the high pressure system has been broken down over central Europe, and in most of Europe ozone levels are now low (Figure 5). However, over northern Europe ozone concentrations are still high.

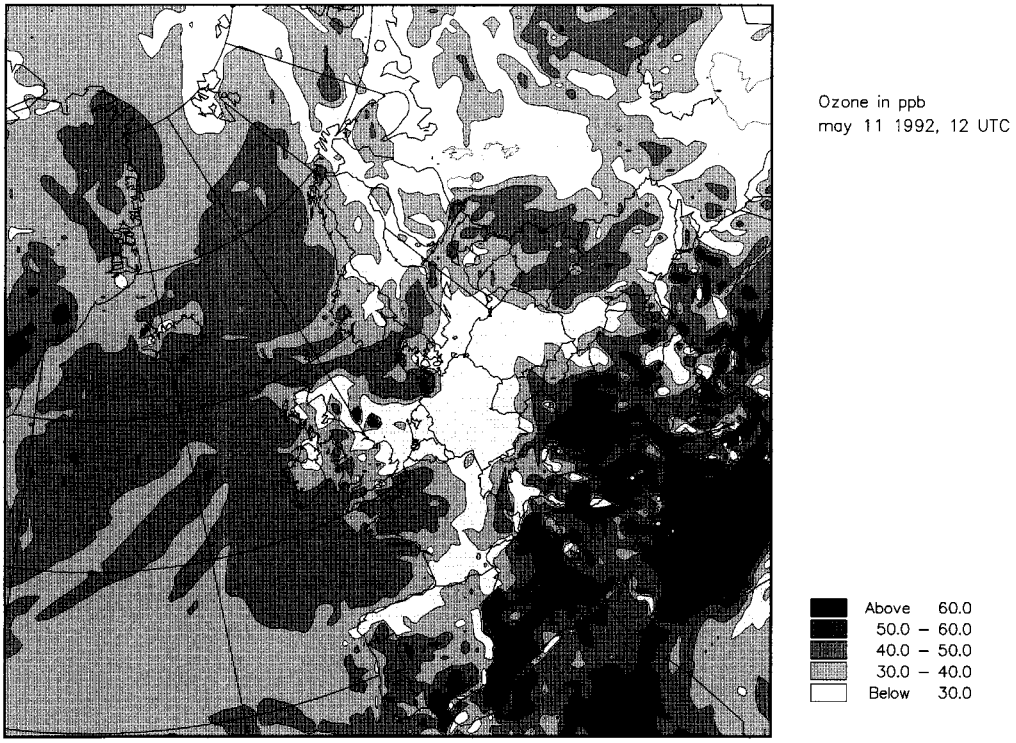

Figure 3 Ozone in ppb_v in the lowest model layer (approx. 45 m) may 11'th 1992 12 UTC

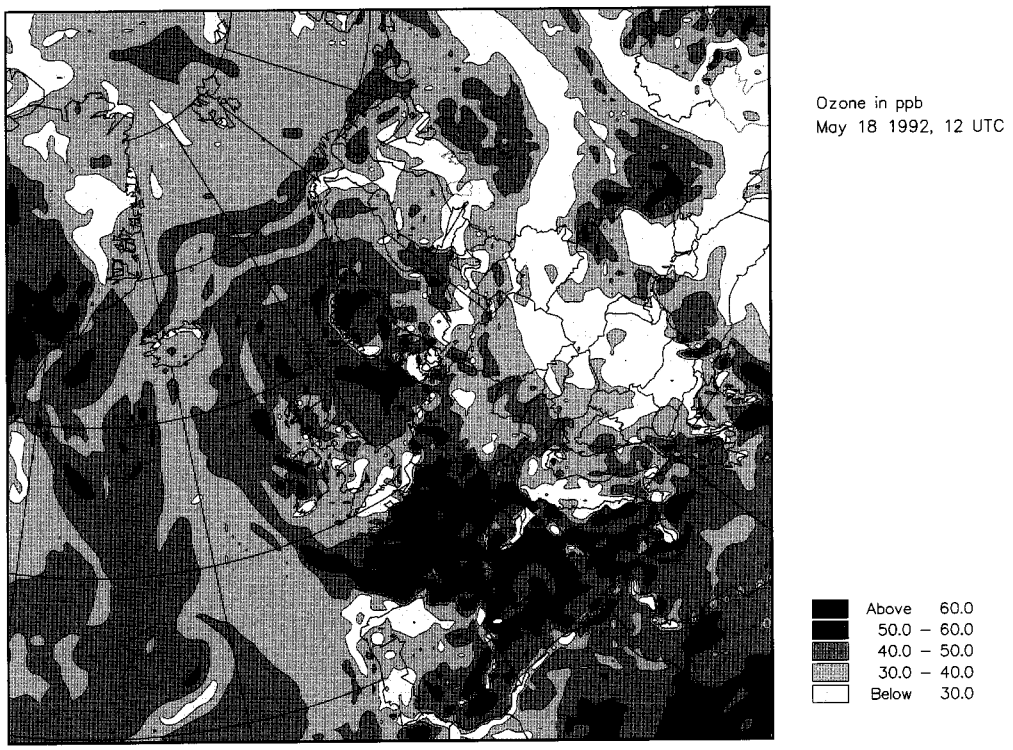

Figure 4 Ozone in ppb_v in the lowest model layer (approx. 45 m) may 18th 1992 12 UTC

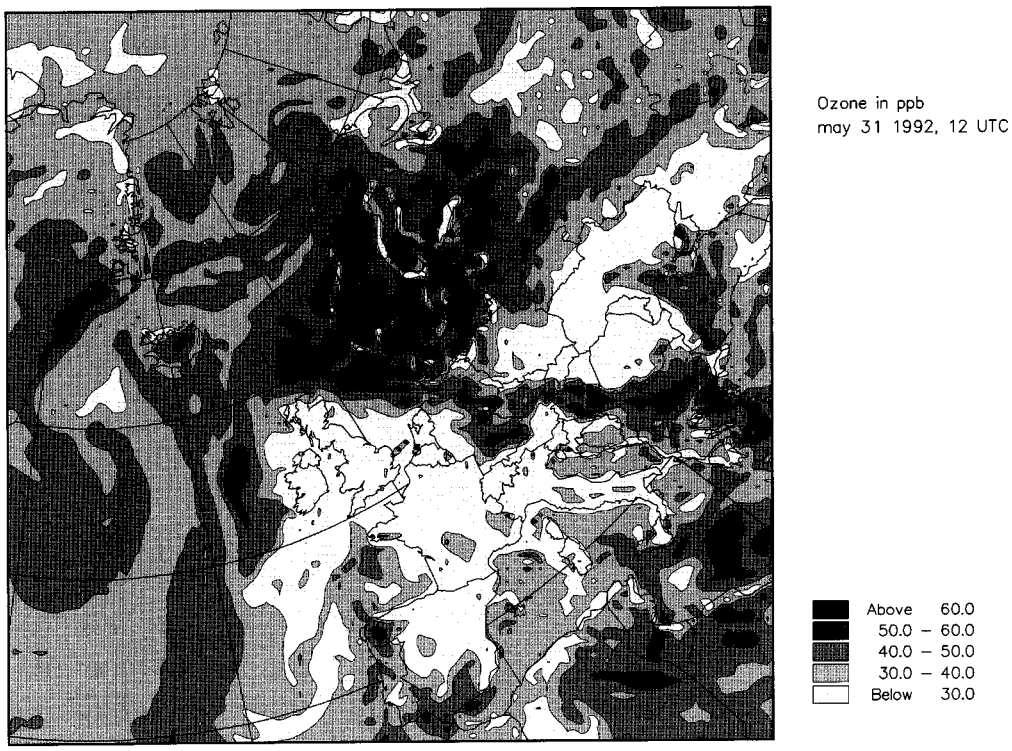

Figure 5 Ozone in ppb_v in the lowest model layer (approx. 45 m) may 31'th 1992 12 UTC

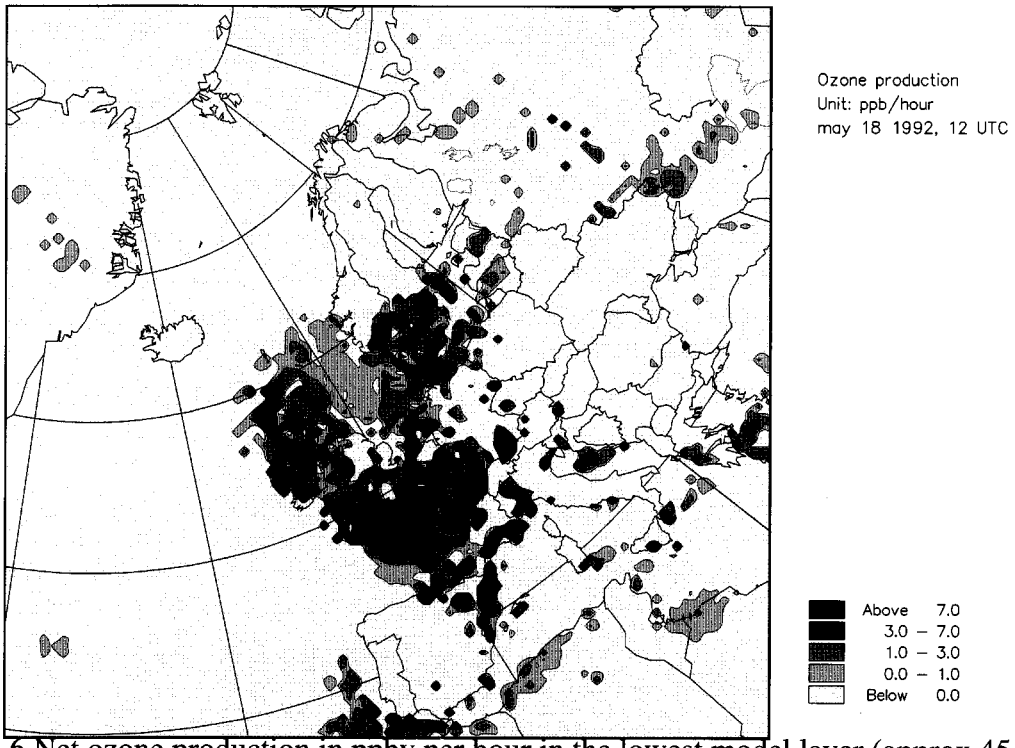

Figure 6 Net ozone production in ppbv per hour in the lowest model layer (approx.45 m) may 18'th 1992, 12 UTC.

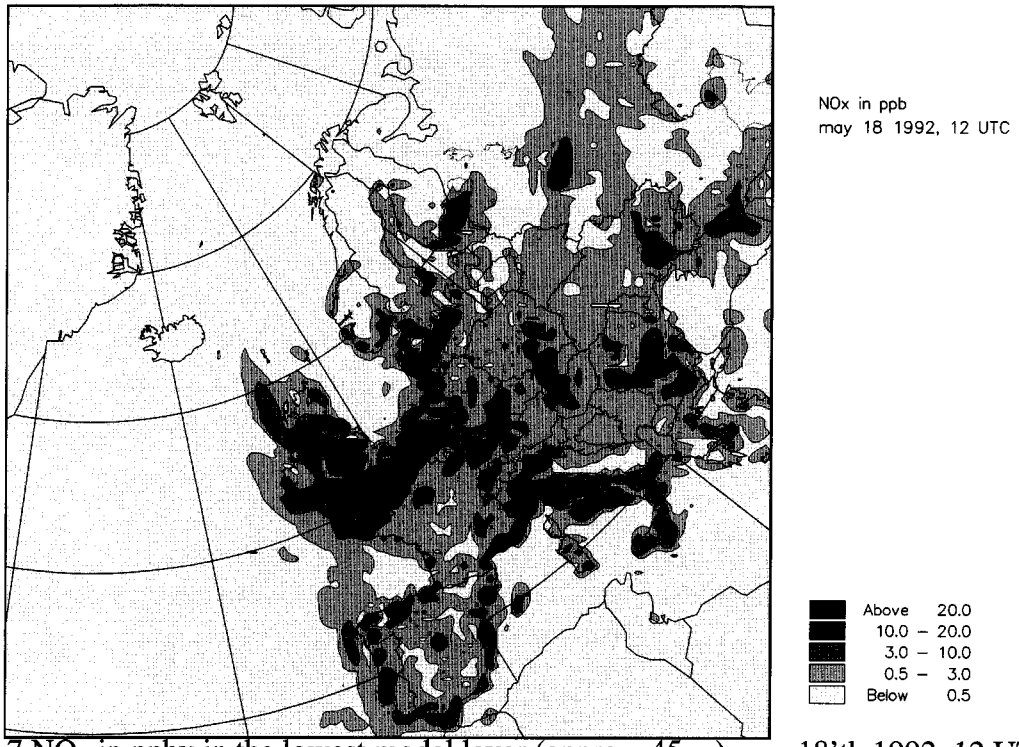

Figure 7 NO_x in ppbv in the lowest model layer (approx. 45 m) may 18'th 1992, 12 UTC

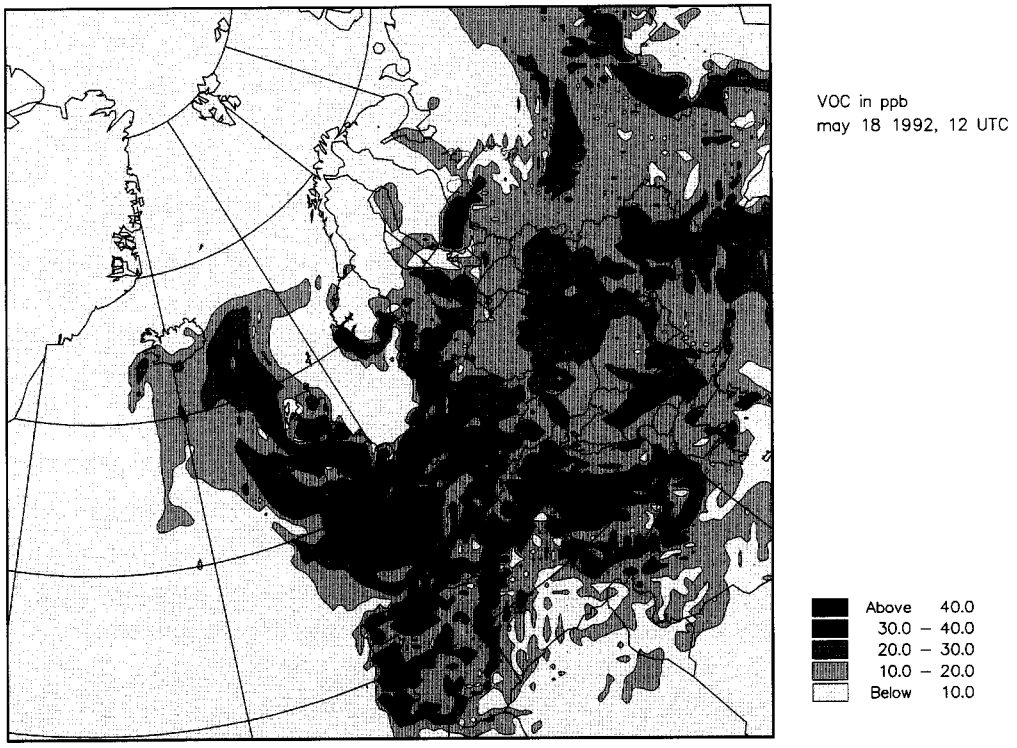

Figure 8 VOC in ppbv in the lowest model layer (approx. 45 m) may 18'th 1992, 12 UTC

4.2 Time series for ozone

In Figures 9 - 11observed and calculated daily maximum ozone values are compared for a limited number of measurement sites. To make the interpretation of the results easier, the sites have been grouped into 3 categories where group 1 includes sites in Scandinavia and Great Britain, group 2 western European sites, and group 3 southern European sites.

In general the model is capable of predicting ozone concentrations and major ozone events quite well. However there is a tendency for the model to underpredict ozone at several sites. In particular this is the case for Ispra in northern Italy. However, as Ispra is situated in valley it is very difficult to simulate the advection of the pollutants and the subsequent buildup of ozone, correctly with a horizontal resolution of 50 km. To some extent the same argument also applies to Schauinsland in the Black Forest.

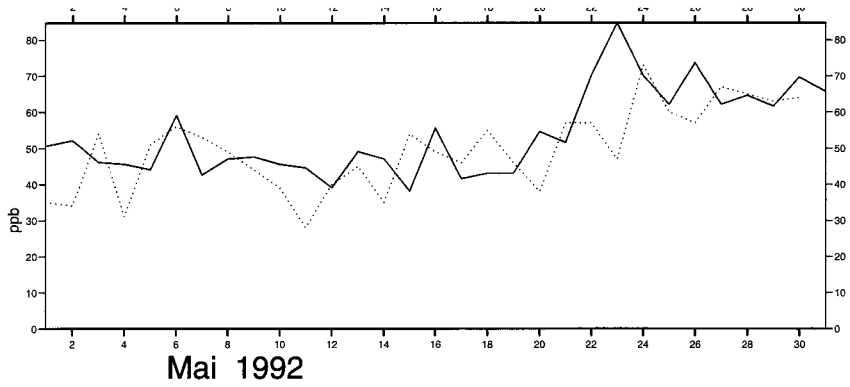

Jeløya (southeast Norway, costal site)

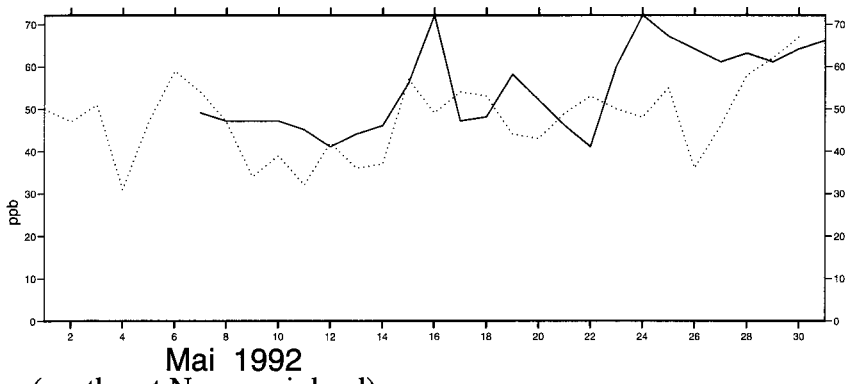

Osen (southeast Norway, inland)

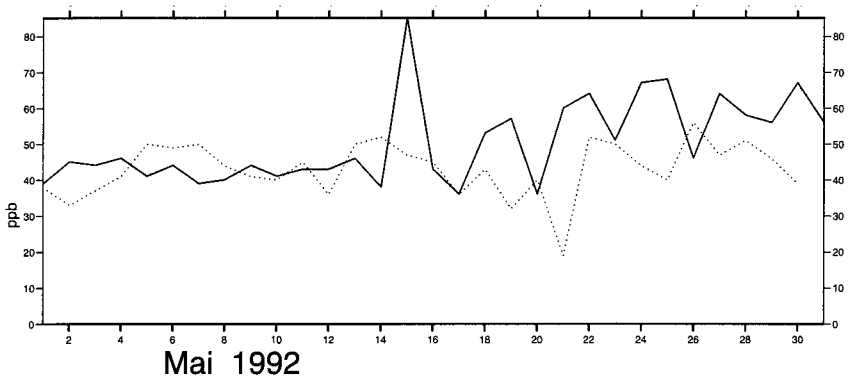

Bush (northern Great Britain)

Figure 9 Measured (full line and calculated (dotted line) daily maximum ozone for sites in Scandinavia and Great Britain.

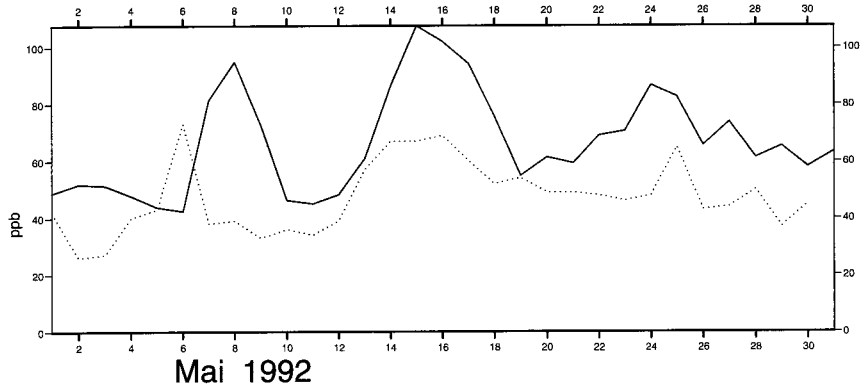

Schauinsland (Black Forest, southern Germany)

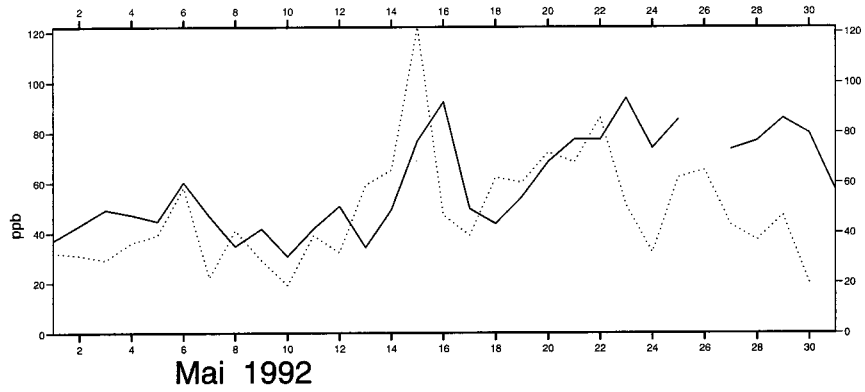

Bilthoven (the Netherlands)

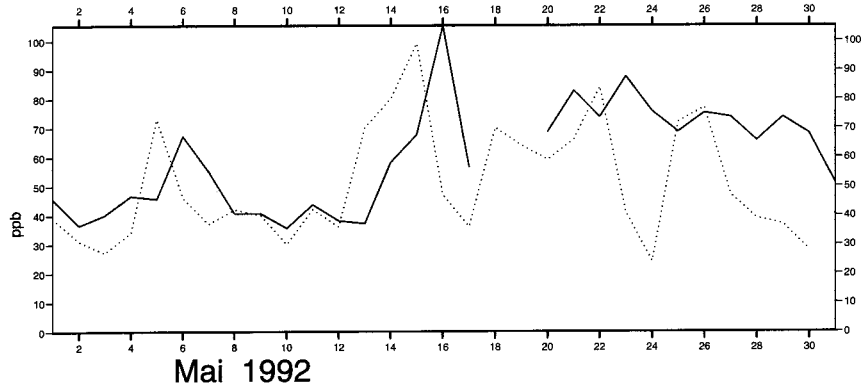

Vredepeel (the Netherlands)

Figure 10 Measured (full line) and calculated (dotted line) ozone for 3 western European sites

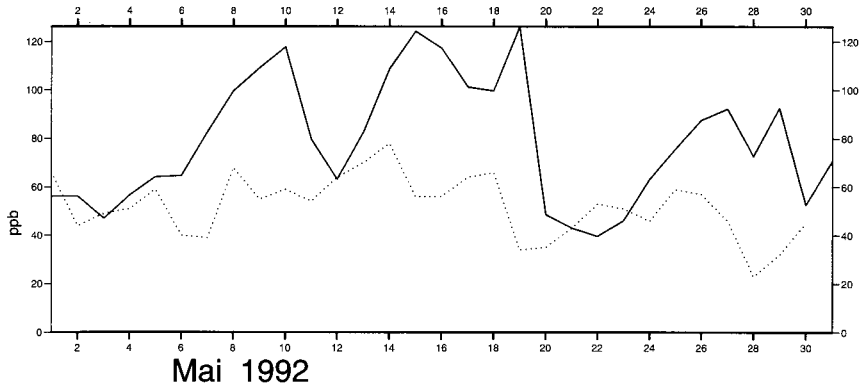

Ispra (northern Italy)

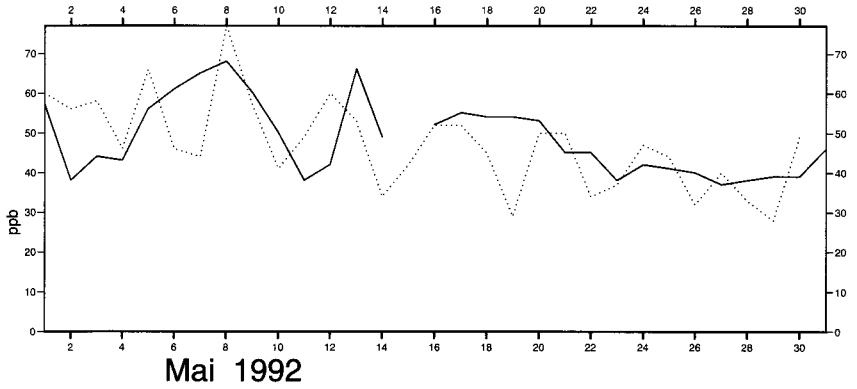

Monte Velho (Portugal)

Figure 11 Measured (full line) and calculated (dotted line) for two southern European sites.

5. Comparisons with the MADE-50 model.

NO_2 and total nitrate (as HNO_3 only in the gas phase in the MACHO model) are calculated both in the MACHO model and in the MADE-50 model (Jakobsen et al. 1997). There are marked differences in the results obtained with the two models. In Figures 12 and 13 calculated and observed monthly averaged NO_2 and total nitrate concentrations are compared for the MACHO model and the MADE-50 model. With the MACHO model calculated average concentrations for both NO_2 and total nitrate are close to the observed values for the 24 sites shown (Figures 12 and 13 respectively). However, for total nitrate (Figure 13) at Scandinavian background sites, far from major sources, total nitrate is in general overpredicted.

Compared to measurements, and to the MACHO model the MADE-50 model tends to under-

predict NO_2 concentrations and overpredict total nitrate concentrations. This strongly suggests that the oxidation of NO_x to total nitrate is to rapid in the MADE-50 model. We believe that in particular the night time oxidation on deliquesent particles is to rapid in the MADE-50 model, but further sensitivity studies must be conducted with the two models to confirm this.

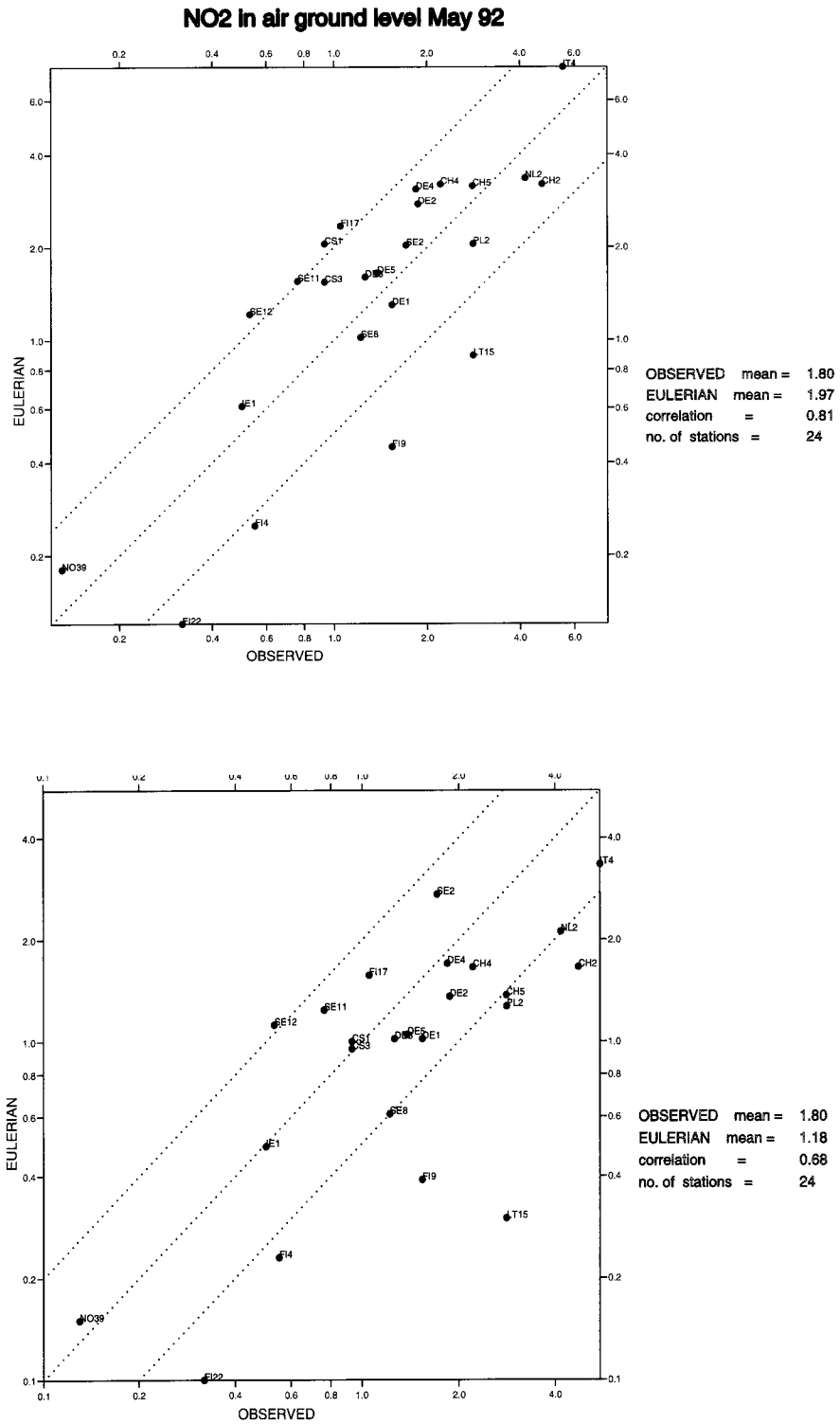

Figure 12 Monthly averaged $NO_{2\,i}$ in $\mu g\ m^{-3}$ calculated by the MACHO model (upper panel), and by the MADE-50 model (lower panel).

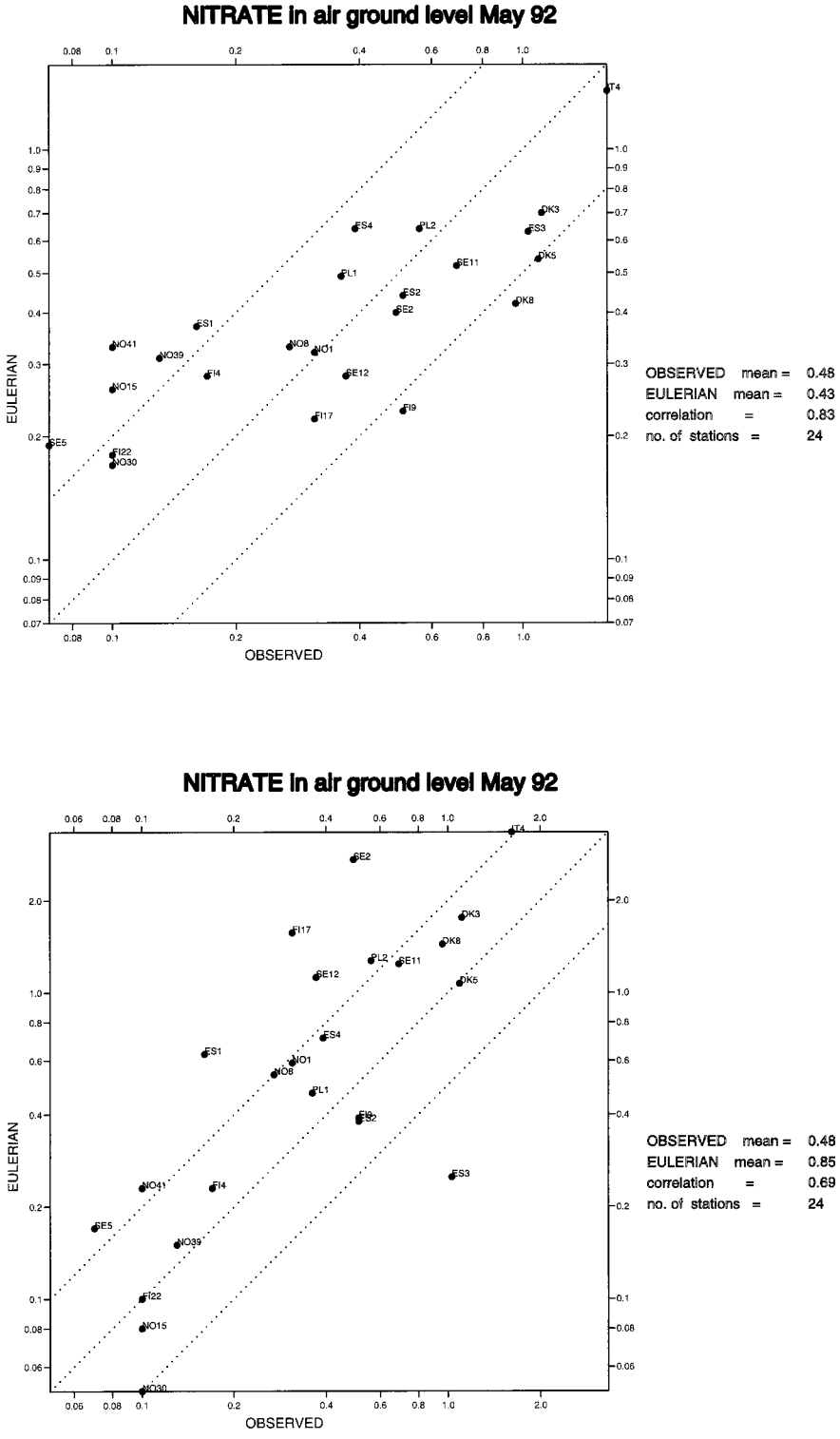

Figure 13 Monthly averaged total nitrate in μg m^{-3} calculated by the MACHO model (upper panel) and by the MADE-50 model (lower panel).

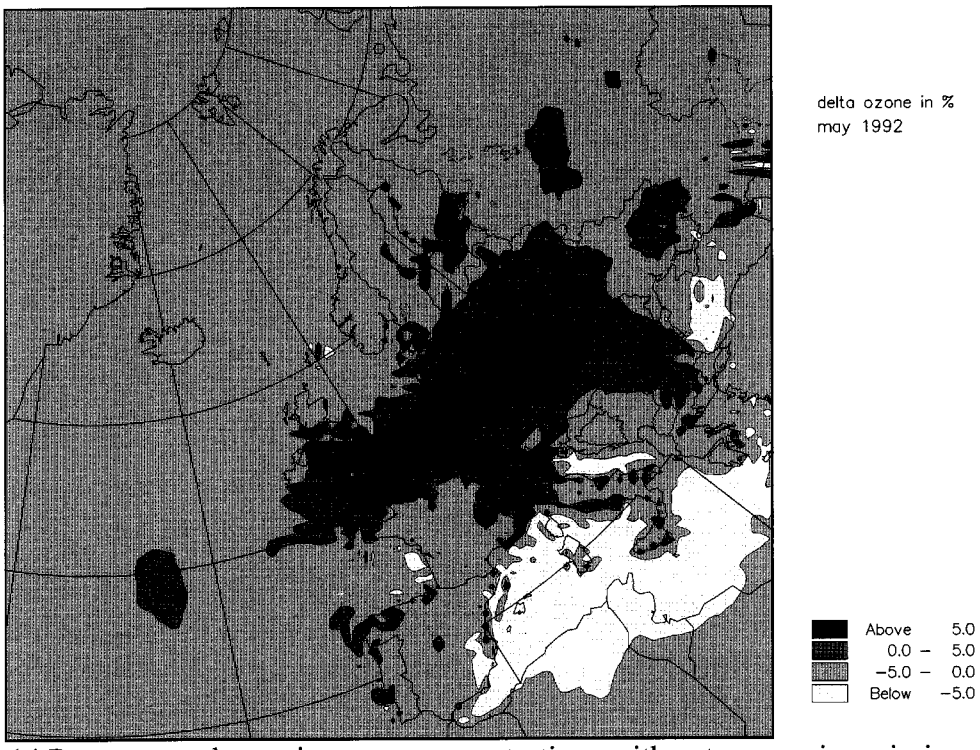

Figure 14 Percentage change in ozone concentrations with antropogenic emissions reduced by 50%, may1992.

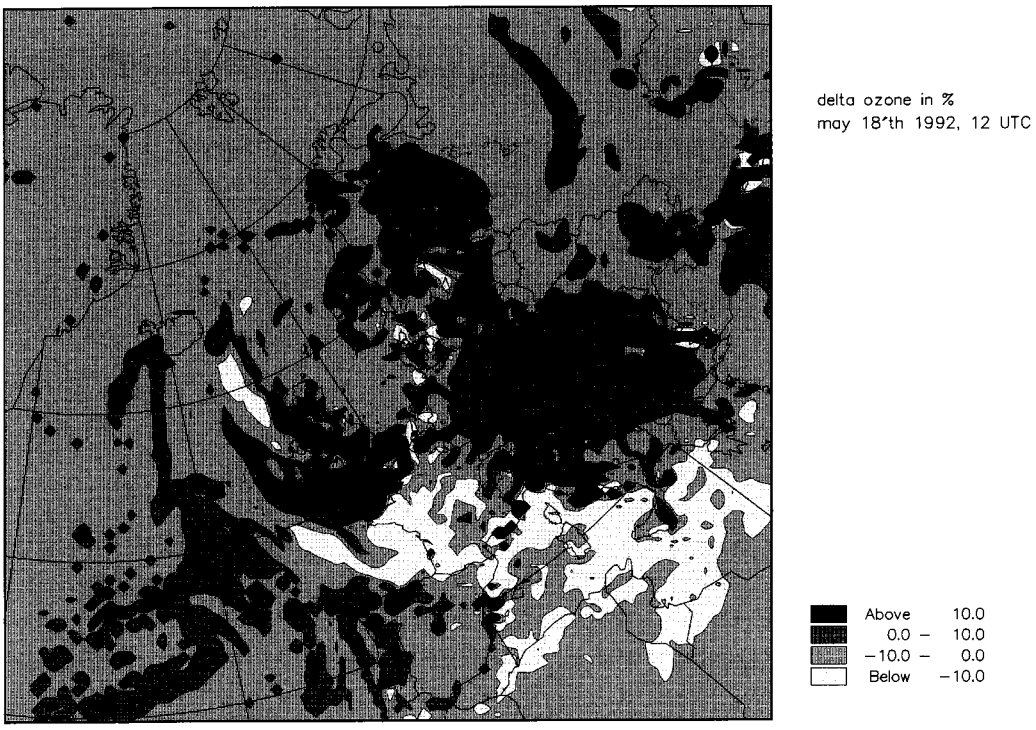

Figure 15 Percentage change in ozone concentrations with antropogenic emissions reduced by 50% may 18'th 1992, 12 UTC.

6 Low emission scenario

Measurements and model calculations indicate that tropospheric ozone has doubled in the free troposphere at northern mid latitudes since the turn of the century (IPCC, 1994 and references therein). In the boundary layer over Europe ozone may have increased even more. The observed increase in ozone concentrations may be attributed to increases in anthropogenic emissions. The formation of ozone is however highly nonlinear. In highly polluted regions with high NO_x concentrations, ozone can be destroyed in reactions with NO_x more rapidly than it can be replenished by local production. In particular at night, when emissions can be trapped in a shallow surface layer, NO_x concentration can build up and subsequently destroy ozone. In Figure 14 the percentage change in ozone concentrations in the lowest model layer for the month of may 1992 between a model run with all emissions included, and a model run where the anthropogenic emissions are divided by two is depicted. In most of the model domain reduced emissions result in a decrease in ozone concentrations. However, throughout large parts of Europe averaged concentrations decrease when emissions are reduced.

In Figure 15 the percentage change in ozone concentrations at 12 UTC, may 18'th for the same model scenarios are shown. A considerable decrease in ozone concentrations can be seen in western parts of France, where ozone concentrations in Figure 4 are high. Over the Netherlands, Belgium and the British Isles, in the pollution plume, where concentrations of NO_x are high, ozone concentrations are increased in the low emission scenario.

Simpson (1993) studied the effects of 50% reductions in ozone emissions for the period April - September 1989. Contrary to our findings, he concluded that reduced emissions would produce rather uniform reductions of ozone throughout Europe of around 10%. The most likely explanation for these, seemingly different conclusions can be that whereas the Lagrangian ozone model applied by Simpson (1993) has one layer only representing the boundary layer, the boundary layer is subdivided into several layers in the MACHO model. As discussed above, NO_x may accumulate in a shallow surface layer at night, destroying ozone. However, as in Simpson (1993) we conclude that reductions in emissions can have a much greater impact in reducing the occurrence of high ozone concentrations throughout Europe as demonstrated for the high ozone event over western parts of France on May 18'th.

7 Summary and conclusions

A first version of a photochemistry model within the framework of the Eulerian multi-layer model system is now in operation. Calculations have been made for one month (May 1992). Comparisons with measurements have been made for several components.

Ozone predicted by the model is in general in good agreement with measurements, and the model is capable of reproducing major ozone events over Europe. Calculated ozone concentrations for some sites are however lower than indicated by the measurements. Overall ozone levels in the model are strongly influenced by influx at the lateral boundaries. Thus, the underprediction of ozone may well be caused by to low ozone levels at the boundaries. Preliminary calculations with the Oslo CTM2 give more ozone (Jostein Sundet, Dep. of Geophysics, University of Oslo). Results from this model will be used at the lateral boundaries and as initial

concentrations in the future.

It is interesting to note that for both NO_2 and total nitrate (HNO_3) calculated concentrations are in much better agreement with measurements than for corresponding calculations performed with the MADE-50 model.

In the future several model updates will be implemented in the MACHO model in order to further improve the results obtained with the model In cooperation with the Department of Geophysics, University of Oslo, a revision of the chemistry is planned, With the revision several differences between the chemistry scheme applied in the MACHO model and the scheme applied in the Lagrangian EMEP ozone model will be removed. To make fully use of the MACHO model as a benchmarking tool for the MADE-50 model, sulphur and ammonia will be included also in the MACHO model. With this extended version multi--pollutant calculations can be performed. Furthermore the dry and wet deposition schemes and the aqueous phase chemistry scheme will be updated to the same level as in the MADE-50 model.

8 References

Barrett K., Seland Ø., Foss A., Mylona S., Sandnes H., Styve H. and Tarason L. (1995) European Transboundary Acidifying Air Pollution: Ten years calculated fields and budgets to the end of the first sulphur protocol. EMEP/MSC-W Report 1/95. The Norwegian Meteorological Institute, Oslo Norway.

Barrett K. and Berge E. (editors) (1996) Transboundary air pollution in Europe. EMEP/MSC-W Status report 1996. The Norwegian Meteorological Institute, Oslo Norway.

Berge E. (1993) Preliminary estimates of sulphur transport and deposition in Europe with a regional scale multi-layer Eulerian Model. EMEP/MSC-W, note 1/93. The Norwegian Meteorological Institute, Oslo Norway

Berntsen T. (1994) Two- and three- dimensional model calculations of the photochemistry of the troposphere. Ph.D. thesis, department of Geophysics, University of Oslo.

Berntsen T. and Isaksen I.S.A. (1997) A global 3D chemical transport model for the troposphere: 1. Model description and CO and O_3 results. Submitted to Journal of Geophys. Res.

Bott, A. (1989a). A positive definite advection scheme obtained by non-linear renormalization of the advective fluxes. Monthly Weather Review, Vol. 117, pp. 1006-1015.

Bott, A. (1989b). Reply on: Comment on a positive definite advection scheme obtained by non-linear renormalization of the advective fluxes. Monthly Weather Review, Vol. 117, No. 11, pp. 2633-2636.

Bott, A. (1992). Monotone flux limitation in the area-preserving flux-form advection algorithm. Monthly Weather Review, Vol. 120, pp. 2592-2602.

Bott, A. (1993). The monotone area-preserving flux-form advection algorithm: Reducing the

time-splitting error in two-dimensional flow fields. Monthly Weather Review, Vol. 121, pp. 2637-2641.

Delfino R.J, Coate B.D., Zeiger R.S., Seltzer J.M., Street D.H. and Koutrakis P. (1996) Daily asthma severity in relation to personal ozone exposure and outdoor fungal spores. *Am. J. of respir. crit. care med.*, Vol. 154, pp 633-641.

Dutsch M.U (1974) The ozone distribution in the atmosphere. *Can. J. Chem.*, Vol. 52, pp 1491-1504.

Easter, R. C. (1993). Two modified versions of Bott's positive-definite numerical advection scheme. Monthly Weather Review, Vol. 121, pp 297-304.

Eliassen A., Hov Ø., Isaksen I.S.A., Saltbones J. and Stordal F. (1982) A Lagrangian long-range transport model with atmospheric boundary layer chemistry. *J. appl. Met.*, Vol. 21, pp 1645-1661.

Gardner R.M., Adams K., Cook T., Deidewig F., Ernedal S., Falk R., Fleuti E. Herms E., Johnson C.E., Lecht M., Lee D.S., Leech M., Lister D., Masse B., Metcalfe M., Newton P., Schmitt A., Vandenbergh C. and VanDrimmelen R. (1997) The ANCAT/EC global inventory of NO_x emissions from aircraft. Atm. Environment, Vol. 31, nr 12, pp 1751-1766

Hestvedt E., Hov Ø. and Isaksen I.S.A. (1978) Quasi steady state approximation in air pollution modelling. Comparison of two numerical schemes for oxidant prediction. Int. Journal of Chem. Kinetics, Vol. X, pp 971-994.

Hjellbrekke A.G. (1995) Ozone measurements 1990-1992. EMEP/CCC Report 4 95. Norwegian Institute for Air Research, Kjeller, Norway

Hov Ø., Stordal F. and Eliassen A. (1985) Photochemical oxidant control strategies in Europe: a 19 day's case study using a Lagrangian model with chemistry. NILU TR 5/85, Norwegian Institute for Air Research.

IPCC (1994) The radiative forcing of climate change. the 1994 report of the scientific assessment group of IPCC.

Jakobsen, H. A., Berge, E., Iversen, T. and Skålin, R. (1995). Status of the development of the multi-layer Eulerian model: a) Model description; b) A new method of calculating mixing heights; c) Model results for sulphur transport and deposition in Europe for 1992 in the 50 km grid. EMEP/MSC-W Note 3/95. The Norwegian Meteorological Institute, Oslo.

Jakobsen, H. A., Jonson, J. E. and Berge, E. (1996). Transport and deposition calculations of sulphur and nitrogen compounds in Europe for 1992 in the 50 km grid by use of the multi-layer Eulerian model. EMEP/MSC-W Note 2/96. The Norwegian Meteorological Institute, Oslo.

Jakobsen, H. A., Jonson, J. E. and Berge, E. (1997). Source receptor relationships for sulphur and nitrogen compounds in Europe for 1992 calculated by use of the multi-layer Eulerian model in the 50 km grid. EMEP/MSC-W Report 2/96. The Norwegian Meteorological Institute, Oslo.

Kley D., Volz A. and Mulheims F. (1988) Ozone measurements in historic perspective. In Tropospheric Ozone - Regional and Global Scale Interactions, edited by I.S.A. Isaksen. NATO ASI Series c, D Reidel, Dordrecht, The Netherlands, Vol. 227, pp 63-72.

Kylling A. (1995) Phodis, a programme for calculation of photodissociation rates in the Earths atmosphere, available by anonymous ftp to kaje@gfi.alaska.edu, cd pub/arve.

Köhler I., Sausen R. and Gallardo Klenner (1995) NO_x production by lightning, in The Impact of NO_x Emissions From Aircraft Upon the Atmosphere at Flight Altitudes 8-15 km (AER-ONOX), edited by U. Schuman, draft, final report to the Commission of the European Communities, Dtsch. Luft und Raumfart Mitt., Oberpfaffenhofen, Germany, pp 343-345.

Malik S., Simpson D., Hjellbrekke A.G. and ApSimpson H. (1996) Photochemical model calculations over Europe for summer 1990. Model results and comparison with observations. EMEP/MSC-W Report 2/95. The Norwegian Meteorological Institute, Oslo.

Simpson D. (1993) Modelling the effects of NO_x and VOC control in Europe: Predictions and uncertainties. In proceedings from EMEP workshop on the control of photochemical oxidants in Europe., edited by Pia Anttila, Finnish Meteorological Institute.

Simpson D., Guenther A., Hewitt C.N. and Steinbrecher R. (1995) Biogenic emissions in Europe. 1. Emissions and uncertainties. J. Geophys. Res., Vol 100, D11, pp 22875-22890.

Stordal F., Isaksen I.S.A. and Horntveth (1985) A diabatic circulation two-dimensional model with photochemistry. Simulations of ozone and long lived tracers with surface sources. *J. Geophys. Res,* Vol. 90, pp 5.757-5.776.

U.S Environmental Protection Agency (1996) Air quality criteria for ozone and related photochemical oxidants. Environmental Protection Agency, Office of Air quality Planning and Standards, Research Triangle Park, North Carolina; EPA //report no. EPA/600/p-93/004bF.

Appendix

Chemical reaction scheme applied in the model. The number in the column labeled ref. refers to the reference for the reaction rates. **1** is DeMore et al., 1990, **2** is Atkinson et al., 1989, **3** is Atkinson 1990, **4** is Vaghjiani and Ravishankara, 1989, **5** is Vaghjiani and Ravishankara, 1991, **6** is DeMore et al., 1992, **7** is Atkinson et al. 1992, **8** is Madronich and Calvert, 1990, **9** is Wayne et al., 1990. and **10** is Dentener and Crutzen, 1993.

nr.	Reactions	Rate constants A	$-E_a/R$	Ref.	Note
R1a	$O(^1D) + M(O_2) \rightarrow O(^3P) + M$	3.2E-11	70	1	
R1b	$O(^1D) + M(N_2) \rightarrow O(^3P) + M$	1.8E-11	110	1	
R2	$O(^1D) + H_2O \rightarrow 2OH$	2.2E-10		1	
R3	$O(^3P) + O_2 + M \rightarrow O_3 + M$		Tab. 2	6	
R4	$O(^3P) + NO_2 \rightarrow NO + O_2$	6.5E-12	120	1	
R5	$O_3 + NO \rightarrow NO_2 + O_2$	2.0E-12	-1400	1	
R6	$O_3 + NO_2 \rightarrow NO_3 + O_2$	1.2E-13	-2450	1	
R7	$O_3 + OH \rightarrow O_2 + HO_2$	1.6E-12	-940	1	
R8	$O_3 + HO_2 \rightarrow OH + 2O_2$	1.1E-14	-500	1	
R9a	$HO_2 + HO_2 \rightarrow H_2O_2 + O_2$	2.3E-13	600	1	
R9b	$HO_2 + HO_2 + M \rightarrow H_2O_2 + O_2 + M$	1.7E-33[M]	1000	1	
R10	$OH + H_2O_2 \rightarrow H_2O + HO_2$	2.9E-12	-160	1	
R11	$OH + NO_2 + M \rightarrow HNO_3 + M$		Tab. 2	6	
R12	$NO + HO_2 \rightarrow NO_2 + OH$	3.7E-12	240	1	
R13a	$NO_2 + NO_3 \rightarrow NO + NO_2 + O_2$	2.5E-14	-1230	6	
R13b	$NO_2 + NO_3 + M \rightarrow N_2O_5 + M$		Tab. 2	6	4
R14	$N_2O_5 + M \rightarrow NO_2 + NO_3 + M$			1	4
R15	$N_2O_5 + aq(aerosol) \rightarrow 2HNO_3(aq)$			10	17
R16	$NO_2 + HO_2 + M \rightarrow HO_2NO_2 + M$		Tab. 2	6	5
R17	$HO_2NO_2 + M \rightarrow HO_2 + NO_2 + M$			1	5

nr.	Reactions	Rate constants A	Rate constants -E_a/R	Ref.	Note
R18	$NO + NO_3 \rightarrow 2NO_2$	1.7E-11	150	1	
R19	$OH + HO_2 \rightarrow H_2O + O_2$	4.8E-11	250	1	
R20	$OH + HNO_3 \rightarrow NO_3 + H_2O$			1	1
R21	$OH + HO_2NO_2 \rightarrow NO_2 + O_2 + HO_2$	1.3E-12	380	1	
R22	$OH + CO + O_2 \rightarrow HO_2 + CO_2$			1	2
R23	$OH + CH_4 \rightarrow CH_3 + H_2O$			5	3
R24	$OH + C_2H_4 \rightarrow CH_3 + CH_2O$		Tab. 2	6	
R25	$O_3 + C_2H_4 \rightarrow HCHO + 0.12HO_2 + 0.44CO$	1.2E-14	-2630	1	
R26	$OH + C_2H_6 \rightarrow C_2H_5O_2 + H_2O$	1.1E-11	-1100	1	
R27	$NO_3 + C_2H_6 \rightarrow C_2H_5O_2 + HNO_3$	5.7E-12	-4426	9	
R28	$OH + C_3H_6 \rightarrow CH_3CH(O_2)CH_2OH$	4.85E-12	504	2	
R29	$O_3 + C_3H_6 \rightarrow 0.25HO_2 + 0.5(CH_2O + CH_3CHO) + 0.15OH + 0.03CH_3O + 0.31CH_3 + 0.07CH_4 + 0.4CO$	6.5E-15	-1900	1	
R30	$OH + C_4H_{10} \rightarrow C_4H_9O_2 + H_2O$			1	6
R31	$OH + C_6H_{14} \rightarrow C_6H_{13}O_2 + H_2O$	5.61E-12		3	
R32	$OH + m\text{-}Xylene \rightarrow 0.6$ AR1	1.04E-11		3	12
R33	$OH + Isoprene \rightarrow ISOR1$	2.54E-11	410	3	13
R34	$CH_3 + O_2 + M \rightarrow CH_3O_2 + M$		Tab. 2	6	
R35a	$CH_3O_2 + CH_3O_2 \rightarrow 0.4 * (2CH_3O + O_2)$	2.2E-13	220	1	
R35b	$\rightarrow 0.6 * CH_2O$			1	
R36	$CH_3O + O_2 \rightarrow HO_2 + CH_2O$	3.9E-14	-900	1	
R37	$OH + CH_2O \rightarrow CHO + H_2O$	1.0E-11	0	1	
R38	$CHO + O_2 \rightarrow HO_2 + CO$	3.5E-12	140	1	
R39	$CH_3O_2 + HO_2 \rightarrow 0.5 * CH_3O_2H + O_2$	3.3E-13	800	1	

nr.	Reactions	Rate constants A	-E_a/R	Ref.	N
R40a	$OH + CH_3O_2H \rightarrow CH_3O_2 + H_2O$	1.79E-12	219	4	
R40b	$OH + CH_3O_2H \rightarrow CH_2O + OH + H_2O$			4	
R41	$OH + AR2 \rightarrow AR3$	2.0E-11		0	1
R42	$OH + ISOK \rightarrow ISOR2$	2.0E-11		0	1
R43	$OH + CH_3COCH_2CH_3 \rightarrow CH_3COCH(O_2)CH_3$				1
R44a	$OH + HCOHCO \rightarrow fa_{44} * (CHO + CO)$	1.1E-11		2	1
R44b	$\rightarrow fb_{44} * (CH_3CO)$				1
R44c	$\rightarrow fc_{44} * (2CO + HO_2)$				1
R45	$OH + RCOHCO \rightarrow CH_3CO + CO$	1.7E-11		3	
R46	$NO + CH_3O_2 \rightarrow fa_{46} * (NO_2 + CH_3O)$	4.2E-12	180	1	
R47	$NO + C_2H_5O_2 \rightarrow fa_{47} * (NO_2 + (1 - fb_{47}) * (CH_2O + CH_3) + fb_{47} * (HO_2 + CH_3CHO))$	4.9E-12	180	1*	8
R48	$NO + C_4H_9O_2 \rightarrow fa_{48} * (NO_2 + (1 - fb_{48}(CH_3CHO + C_2H_5O_2) + fb_{48} * (HO_2 + CH_3COCH_2CH_3))$	4.9E-12	180	1*	
R49	$NO + C_6H_{13}O_2 \rightarrow fa_{49} * (NO_2 + C_4H_9O_2 + CH_3CHO)$	4.9E-12	180	1*	1
R50	$NO + AR1 \rightarrow NO_2 + HO_2 + AR2 + RCOHCO$	4.2E-12	180	1**	1
R51	$NO + AR3 \rightarrow NO_2 + HO_2 + HCOHCO + RCOHCO$	4.2E-12	180	1**	1
R52	$NO + ISOR1 \rightarrow fa_{52}(NO_2 + HO_2 + ISOK + CH_2O)$	4.2E-12	180	1**	1
R53	$1.5NO + ISOR2 \rightarrow 1.5NO_2 + 0.67HO_2 + 0.43CH_2O + 0.67RCOHCO + 0.33CH_3CO + 0.33CH_3CHO$	4.2E-12	180	1**	1
R54	$NO + CH_3COCH(O_2)CH_3 \rightarrow fa_{54} * (NO_2 + HO_2 + CH_3COCOCH_3)$	4.2E-12	180	1**	
R55	$NO + CH_3CH(O_2)CH_2OH \rightarrow NO_2 + CH_2O + CH_3CHO + HO_2$	4.2E-12	180	1**	
R56	$OH + CH_3CHO \rightarrow CH_3CO + H_2O$	6.0E-12	250	1	
R57	$NO_3 + CH_3CHO \rightarrow HNO_3 + CH_3CO$	1.2E-12	-1860	7	

* Rate assumed to be 1.16 times faster than R46, as Atkinson et al. (1989) gives k_{298} 1.16 times faster for $C_2H_5O_2 + NO$ than for $CH_3O_2 + NO$.

** Rate assumed to be equal to R46 ($NO + CH_3O_2$)

Rate constants for three-body reactions.

Reaction	Rate constants k_0	k_{inf}	F_c
R3	6.0E-34$(T/300)^{-2.3}$[M]		
R11	2.6E-30$(T/300)^{-3.2}$[M]	2.4E-11$(T/300)^{-1.3}$	0.6
R13b	2.2E-30$(T/300)^{-3.9}$[M]	1.5E-12$(T/300)^{-0.7}$	0.6
R16	1.8E-31$(T/300)^{-3.2}$[M]	4.7E-12$(T/300)^{-1.4}$	0.6
R24	1.0E-28$(T/300)^{-0.8}$[M]	8.8E-12	0.6
R34	4.5E-31$(T/300)^{-3.0}$[M]	1.8E-12$(T/300)^{-1.7}$	0.6
R60	8.0E-29$(T/300)^{-7.0}$[M]	1.2E-11$(T/300)^{-1.0}$	0.6
R61	4.9E-3$e^{(-12100/T)}$[N_2]	4.0E+16$e^{(-13600/T)}$	0.3

Note 1 : $k = k_0 + k_3[M]/(1 + k_3[M]/k_2)$
where $k_0 = 7.2 \times 10^{-15} exp(785/T)$, $k_2 = 4.1 \times 10^{-16} exp(1440/T)$ and $k_3 = 1.9 \times 10^{-33} exp(725/T)$

Note 2 : $1.5 \times 10^{-13}(1.0 + 0.6P_{atm})$
where P_{atm} is air pressure in atmospheres.

Note 3 R23: $k = 1.59 * 10^{-20} * T^{2.84} * e^{-984/T}$

Note 4 : Equilibrium constant. for $NO_2 + NO_3 \rightarrow N_2O_5$ is $k_{eq} = 4.0E - 27e^{(10930./T)}$. Reaction rate for $N_2O_5 \rightarrow NO_2 + NO_3$ is then given as R13b/k_{eq} .

Note 5 : Equilibrium const. for $HO_2 + NO_2 \rightarrow HO_2NO_2$ is $k_{eq} = 2.1E - 27e^{(10900./T)}$. Reaction rate for $HO_2NO_2 \rightarrow HO_2 + NO_2$ is then given as R16/k_{eq} .

Note 6 R30 : $k = 1.51 * 10^{-17} * T^{2.0} * e^{190/T}$

Note 7 R40a + R40b= $2.93E - 12 * e^{190/T}$, R40b = $2.93E - 12 * e^{190/T}$-R40a

Photolytic reactions

Model ref.	Reactions
D1	$O_3 + h\nu \rightarrow O(^3P) + (O_2)$
D2	$O_3 + h\nu \rightarrow O(^1D) + (O_2)$
D3	$NO_2 + h\nu \rightarrow NO + O(^3P)$
D4	$H_2O_2 + h\nu \rightarrow 2OH$
D5	$HNO_3 + h\nu \rightarrow NO_2 + (OH)$
D6	$HCHO + h\nu \rightarrow CHO + HO_2$
D7	$HCHO + h\nu \rightarrow CO + (H_2)$
D8	$CH_3CHO + h\nu \rightarrow CHO + CH_3$
D9	$CH_3COCH_2CH_3 + h\nu \rightarrow CH_3CO + C_2H_5O_2$
D10	$CH_3COCOCH_3 + h\nu \rightarrow 2CH_3CO$
D11	$HCOCHO + h\nu \rightarrow CO + HCHO$
D12	$CH_3COCHO + h\nu \rightarrow CO + CH_3CHO$
D13	$NO_3 + h\nu \rightarrow NO_2 + O(^3P)$
D14	$NO_2NO_3 + h\nu \rightarrow NO_2 + NO_3$
D15	$CH_3O_2H + h\nu \rightarrow OH + CH_3O$
D16	$HO_2NO_2 + h\nu \rightarrow NO_2 + HO_2$

Note 8 The fraction $(1 - fa, fa = k_b/k_a + k_b)$ of organic nitrates ($RONO_2$) formed from the reaction RO_2 + NO $\longrightarrow$ (1-fa)$RONO_2$ +fa(NO_2 + TO) is calculated by the following equations (Atkinson, 1990)

$$\frac{k_a}{k_b} = \left\{ \frac{Y_0^{300}[M](T/300)^{-m_0}}{1 + \frac{Y_0^{300}[M](T/300)^{-m_0}}{Y_\infty^{300}[M](T/300)^{-m_\infty}}} \right\} F^z$$

$$z = \left[1 + \left(log_{10} \frac{Y_0^{300}[M](T/300)^{-m_0}}{Y_\infty^{300}[M](T/300)^{-m_\infty}} \right)^2 \right]^{-1}$$

where $Y_0^{300} = \alpha e^{\beta N}$, where N is the number of C atoms in the peroxy radical, and $\alpha = 1.94 * 10^{-22}$ and $\beta = 0.97$ are constants. $[M]$ is number density of the air, T is temperature and $m_0 = 0$, $m_\infty = 8.1$, $F = 0.411$ and $Y_\infty^{300} = 0.826$.

Note 9 The alkoxy radicals (RO) formed in the reaction between peroxy radical and NO will either react with O_2 or decompose. Values of fb (fb denotes the fraction reacting with O_2) are calculated on the basis of data given in Atkinson (1990).

Note 10 In the case of $C_6H_{13}O$, decomposition is assumed to be the only reaction since a C6 ketone is not included in the scheme.

Note 11 ARAD is the sum of peroxy radicals (ARAD = $CH_3COCH(O_2)CH_3 + C_6H_{13}O_2 + C_4H_9O_2 + C_2H_5O_2 + CH_3CH(O_2)CH_2OH + ISOR1 + ISOR2$). All reactions are assumed to give a $ROOH$ compound which is represented in the scheme by CH_3O_2H.

Note 12 List of abbreviations used in the chemical scheme :

ISOR1	First RO_2 radical from the reaction of isoprene with OH
ISOK	The sum of methylvinylketone (MVK) and methacrolein (MACR)
ISOR2	RO_2 radical formed from MVK + OH or MACR + OH
AR1	First RO_2 radical from the reaction of m-xylene with OH
AR2	A C-5 carbonyl compound formed from AR1 by reaction R50
AR3	A C-5 RO_2 radical formed from AR2 by R41

Note 13 The scheme for isoprene oxidation is based on Lloyd et al. 1983. Since the uncertainties in the emission estimates are so large only oxidation initialized by reaction with OH is included. The scheme based on assumptions I-III is :

Isoprene + OH $\longrightarrow$ ISOR1

ISOR1 + NO $\longrightarrow$ 0.1 $RONO_2$ + 0.9 (NO_2 + HO_2 + HCHO + ISOK) I

ISOK + OH $\longrightarrow$ ISOR2 II

ISOR2 + 1.5 $NO \longrightarrow 1.5NO_2 + 0.67\ (HO_2 + CH_3COHCO) + 0.43\ HCHO$
$+0.33(CH_3CHO + CH_3CO\ )$ III

I : ISOK consists of equal amounts of MVK and MACR.

II : MVK and MACR have the same chemical lifetime.

III : All RO_2 radicals in ISOR2 reacts with the same rate with NO.

In Lloyd et al. (1983) 4 different RO_2 radicals are identified from the reaction of ISOK with OH depending on whether MVK or MACR is oxidized, and the mechanism for the oxidation. The fraction yields of the products in the last equation is derived by considering the fraction yields of the 4 RO_2 radicals and their reaction path to the above products. A simplification is made as the $HOCH_2CO$ radical formed from one of the RO_2 radicals formed from MVK, is treated as CH_3CO in the scheme.

Note 14 Product yields of the reaction of OH with glyoxal is given by Atkinson (1990) as

$$k_a/k = fa_{44} = \frac{3.5 * 10^{18}}{3.5 * 10^{18} + 2 * [O_2]}$$

$$k_b/k = fb_{44} = \frac{[O_2]}{3.5 * 10^{18} + 2 * [O_2]}$$

$$k_c/k = fc_{44} = fb_{44}$$

Note 15 $k = 3.2 * 10^{-18} * T^2 * e^{414/T}$, Atkinson 1990.

Note 16 Products taken from Madronich and Calvert (1990). The alkoxy radicals which are products of the reaction are treated according to note 9.

Note 17 Pseudo first order reaction rates ,$\overline{k}(\phi, z)$, (zonally and yearly averaged) are taken from calculations by Dentener and Crutzen, 1993.

$$k(\lambda, \phi, z, month) = \overline{k}(\phi, z) + k'$$

k' is parameterized by :

$$k' = f(\phi) \times g(month) \times \overline{k}(\phi, z)$$

$$f(\phi) = (COS(2\phi + \pi) + 1)/2$$

$$g(month) = 0.8 \times COS(\frac{month + 6}{12} \times 2\pi) \qquad Northern\ Hemisphere$$

$$g(month) = 0.8 \times COS(\frac{month}{12} \times 2\pi) \qquad Southern\ Hemisphere$$